J Mol Model (2013) 19:4877–4886
DOI 10.1007/s00894-013-1978-6

ORIGINAL PAPER

Exploring surface reactivity of phosphorous-doped (6,0) and (4,4) BC3 nanotubes: a DFT study

Mohammad Alizadeh · Mehdi D. Esrafili · Esmail Vessally

Received: 12 June 2013 / Accepted: 21 August 2013 / Published online: 17 September 2013

Abstract We report a density functional theory study on the electronic structure properties of pristine and phosphorous-doped (6,0) and (4,4) single-walled BC3 nanotubes (BC3NTs). We examine the usefulness of local reactivity descriptors to predict the reactivities of different carbon/boron atomic sites on the external surface of the tubes. Electrostatic potentials $V_S(\mathbf{r})$ and average local ionization energies $\bar{I}_S(\mathbf{r})$ are computed on the surface of the investigated BC3NTs. A general feature of the systems considered here is that the magnitudes of negative $V_S(\mathbf{r})$ associated with carbon atoms tend to be stronger when the boron atom is substituted with a phosphorous atom. In order to verify the surface reactivity pattern based on the chosen reactivity descriptors, we calculated the reaction energies for the interaction of an H^+ ion or H radical with external surface of the (6,0) and (4,4) BC3NTs. It is clear that, for each nanotube studied, the reaction energies correlate well with the values of $V_S(\mathbf{r})$ and $\bar{I}_S(\mathbf{r})$.

Keywords BC3 nanotubes · Electrostatic potential · Average local ionization energies · Reaction energies

Introduction

In recent years, carbon nanotubes (CNTs) have stimulated remarkable research interest in many scientific fields due to their outstanding mechanical and electronic properties [1–6]. Their perfect hollow structures have excited chemists to renovate traditional adsorption and catalysis materials and, actually, it has been proved that they can significantly promote the adsorption of energy molecules [7, 8] and modulate molecular reactivity and selectivity [9, 10]. Modification of the properties of CNTs by controllably placing defects or hetero-atoms brings along tremendous technological implications, which justifies the number of experimental and theoretical investigations focused on this topic [11–15]. It was found that doping CNTs with other elements like B can efficiently tailor their electronic and mechanical properties [16], which might lead to some novel applications. Therefore, carbon-based nanotubes such as BC3 have also been reported theoretically [17–19] and synthesized experimentally [20–22]. Like CNTs, BC3 nanotubes (BC3NTs) can be formed structurally by rolling a BC3 sheet along the chiral vector. However, on BC3NTs, there are only B–C and C–C chemical bonds and the less stable B–B bonds are excluded [23]. According to theoretical results [24], the formation energies of pure CNTs are slightly greater than those of BC3NTs, as compared to a graphene layer, it is easier to roll a BC3 sheet into a tube.

The possible use of CNTs and other carbon-based nanotubes as detectors for gas molecules attracts much attention at present due to the high values of adsorbing area and sensitivity of such materials to adsorbed molecules [25–27]. By means of suitable chemical doping, CNTs can exhibit different electronic properties in gas sensitivity and hydrogen storage, which will broaden the nanotube's application fields to a great extent [28–30]. However, these interactions, such as physical adsorption, are attributed mainly to electrostatic effects [31, 32]. In order to provide some insightful information into the origin of physisorption processes, it is essential to characterize in detail the local reactivity descriptors. Previously, Politzer and co-workers have developed several statistically defined quantities that provide clear insights into the

M. Alizadeh
Deputy of Enviroment, Tehran, Iran

M. D. Esrafili (✉)
Laboratory of Theoretical Chemistry, Department of Chemistry, University of Maragheh, PO Box 5513864596 Maragheh, Iran
e-mail: esrafili@maragheh.ac.ir

E. Vessally
Department of Chemistry, Payame Noor University, Tehran, Iran

chemical reactivity and regioselectivity of molecules based on local reactivity indexes [33, 34]. These local indexes include the magnitudes of electrostatic potential, $V(\mathbf{r})$, and average local ionization energy, $\bar{I}(\mathbf{r})$, at each point on the molecular surface. Recent studies [35–38] indicate that different subsets of these indexes can be used to develop analytical representations of good accuracy for a variety of solution, liquid and solid phase properties that depend upon noncovalent interactions. Moreover, this approach was applied to interactions in a group of CNTs, boron–nitride nanotubes (BNNTs) and silicon–carbide nanotubes (SiCNTs) as well as fullerenes [39–43]. A qualitative correlation with free energies of solvation indicated that the BNNTs should have considerably greater water solubilities [40]. Recently [44], the relative reactivities of various carbon atomic sites of zigzag and armchair CNTs, either with and without a Stone-Wales defect, have analyzed using the local ionization energies $\bar{I}_S(\mathbf{r})$. For the (5,5) armchair CNT, it was revealed that the lowest $\bar{I}_S(\mathbf{r})$, predicted to indicate the most reactive carbon, is for one that shares five-, six- and seven-membered rings. Leszczynski and co-workers [45] indicated that the minimum values of $\bar{I}_S(\mathbf{r})$ correlate well with the computed reaction energies for the addition of a second chlorine radical on the external surface of monochloro-(5,5) armchair single-walled carbon nanotubes (SWCNTs).

In this work, we report the results of density functional theory (DFT) calculations on the surface reactivity of representative models of zigzag (6,0) and armchair (4,4) BC3NTs. The reactivities of different carbon/boron atoms in the BC3NTs were examined using the computed surface electrostatic potentials, $V_S(\mathbf{r})$ and average local ionization energies $\bar{I}_S(\mathbf{r})$. Our major question is aimed at understanding the influence of tube chirality as well as the phosphorous-doping effect on the surface reactivity of the BC3NTs. The relative reactivities of the carbon/boron atoms will be verified *via* calculated reaction energies for a single hydrogen atom and H^+ cation chemisorptions on the external surfaces of the tubes.

Computational aspects

All quantum chemistry calculations were carried out with the DFT framework as implemented in the GAMESS suite of programs [46]. We performed DFT calculations employing the B3LYP hybrid functional and the 6-31G* standard basis set to investigate the electronic structure properties of the representative (6,0) zigzag and (4,4) armchair BC3NTs (Fig. 1). Both ends of the truncated BC3NTs were capped with hydrogen atoms to saturate dangling bonds. The B3LYP/6-31G* optimized structures were used to compute the $V_S(\mathbf{r})$ and $\bar{I}_S(\mathbf{r})$ quantities over grids covering both the inner and outer 0.001 au surfaces of the tubes. The surface electrostatic potentials and $\bar{I}_S(\mathbf{r})$ quantities were computed at the same level using the WFA code of Bulat et al. [33].

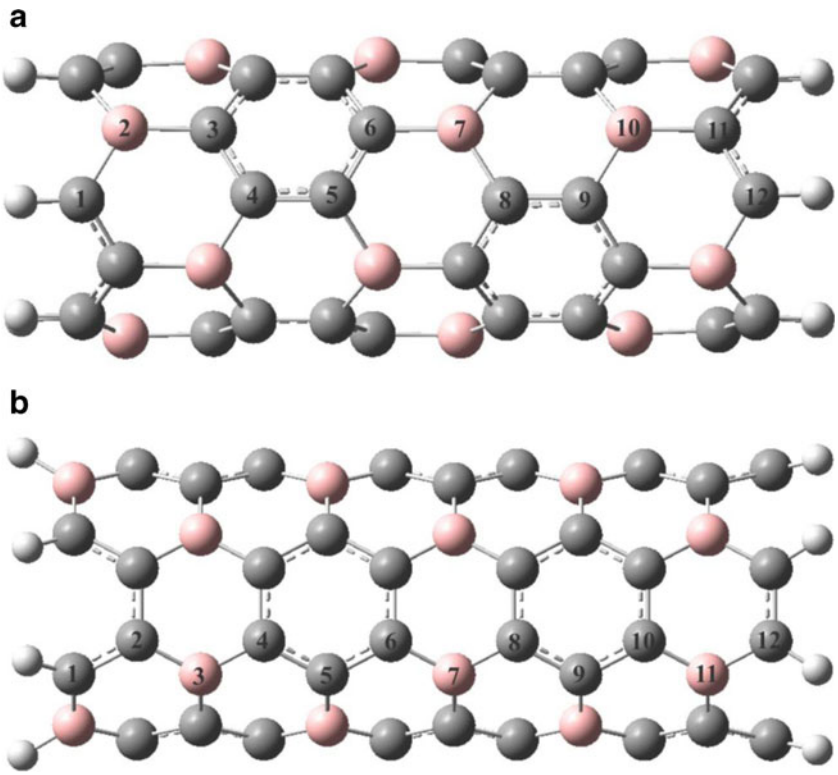

Fig. 1 Structure and atomic numbering scheme for **a** pristine (6,0) BC3NT and **b** pristine (4,4) BC3NT

The electrostatic potential V(**r**) that the electrons and nuclei of a molecule create at any point **r** in surrounding space is given by [47]:

$$V(\mathrm{r}) = \sum_A \frac{Z_A}{|R_A - \mathrm{r}|} - \int \frac{\rho(\mathrm{r}')d\mathrm{r}'}{|\mathrm{r}' - \mathrm{r}|} \quad (1)$$

in Eq. (1), Z_A refers to the charge on nucleus A, located at R_A, and $\rho(\mathbf{r})$ stands for the molecule's electronic density. V(**r**) in a given point can be positive or negative, depending upon whether the contribution of the nuclei or that of the electrons is dominant there. In using V(**r**) to predict interactive tendencies, they are generally computed on the surface of the molecule and the results are labeled $V_S(\mathbf{r})$. We take this to be the 0.001 electrons/bohr^3 contour of the electronic density $\rho(\mathbf{r})$, according to Bader et al. [45]. $V_S(\mathbf{r})$ is suitable for noncovalent interactions, which are essentially electrostatic in nature. More especially, the electrostatic potential maxima ($V_{S,max}$) indicate the sites favored for a nucleophilic attack, whereas the minima ($V_{S,min}$) correspond to the sites susceptible for an electrophilic attack [47]. In contrast to V(**r**), the average local ionization energy, $\bar{I}(\mathbf{r})$, is interpreted as a means of estimating the sites of the more reactive electrons in a molecule, and is given by [48, 49]:

$$\bar{I}(\mathrm{r}) = \frac{\sum_i \rho_i(\mathrm{r})|\varepsilon_i|}{\rho(\mathrm{r})} \quad (2)$$

Here, $\rho_i(\mathbf{r})$ is the electronic density of the i^{th} occupied atomic or molecular orbital and ε_i is its energy. $\bar{I}(\mathbf{r})$ gives the average energy required to remove an electron at the point **r**, with the focus being on the point in space rather than on a particular orbital. Like $V_S(\mathbf{r})$, the computed $\bar{I}(\mathbf{r})$ are evaluated on the molecular surface and labeled $\bar{I}_S(\mathbf{r})$. The minima of $\bar{I}_S(\mathbf{r})$, $\bar{I}_{S,min}$, correspond to the least tightly held electrons, which should be the sites most reactive to electrophilic or to free radical attack [48, 49].

In order to characterize the electrostatic potential quantitatively over the entire molecular surface, several statistically defined global quantities may be useful, among which are the following [50]:

(1) The positive, negative and overall average potentials on the surface:

$$\overline{V_S^+} = \frac{1}{m}\sum_{i=1}^{m} V_S^+(\mathrm{r}_i) \quad , \quad \overline{V_S^-} = \frac{1}{n}\sum_{i=1}^{n} V_S^-(\mathrm{r}_i), Vs$$
$$= \frac{1}{m+n}\left(\sum_{i=1}^{m} V_S^+(\mathrm{r}_i) + \sum_{i=1}^{n} V_S^-(\mathrm{r}_i)\right) \quad (3)$$

Here, the summations are over the m positive and n negative points of a square surface grid, with $\overline{V_S^+}$ and $\overline{V_S^-}$ being their averages.

(2) The average deviation of $V_S(\mathbf{r})$:

$$\Pi = \frac{1}{m+n}\sum_{i=1}^{m+n}\left|V_S(\mathrm{r}_i) - \overline{V_S}\right| \quad (4)$$

Π is interpreted as an indicator of the internal charge separation in any molecule and is present even in molecules that have zero dipole moments [51].

and (3) The total variance of $V_S(\mathbf{r})$, σ_{total}^2:

$$\sigma_{total}^2 = \sigma_+^2 + \sigma_-^2 = \frac{1}{\alpha}\sum_{j=1}^{\alpha}\left[V_S^+(\mathrm{r}_j) - \overline{V_S}^+\right]^2 + \frac{1}{\beta}\sum_{k=1}^{\alpha}\left[V_S^-(\mathrm{r}_k) - \overline{V_S}^-\right] \quad (5)$$

Results and discussion

The finite-size pristine and P-doped models of the representative (6,0) zigzag and (4,4) armchair BC3NTs are illustrated in Fig. 1. In order to investigate the effect of phosphorous impurity on the electronic properties of the pristine BC3NTs, three different doping configurations were considered. Model P_{B7} stands for the P-doped BC3NT, in which one boron atom (at the site of B7) is substituted by a single P atom. Models P_{C6} and P_{C8} stand for the P-doping at the sites of C6 and C8, respectively. The criterion for doping only one atom was intended to keep only a traceless concentration of dopant in the investigated structures of BC3NTs. In the following sections, we will compare different models of pristine and P-doped BC3NTs from structural and surface reactivity properties points of view and show how these individual parameters can be used to ascertain the relative reactivity trends in the pristine/P-doped BC3NTs.

(6,0) zigzag BC3NTs

The structure and numbering scheme of pristine and P-doped zigzag BC3NTs are illustrated in Figs. 1 and 2. For the pristine (6,0) zigzag nanotube, the nonequivalent lengths for B–C and C–C bonds are 1.57 and 1.42 Å, respectively. Geometry optimizations reveal that the shape of the cross-section of the P-doped nanotubes changes from circular to slightly oval. The tube diameter at the defect site is about 5.6 Å, and the phosphorus atom protrudes outwardly from the nanotube

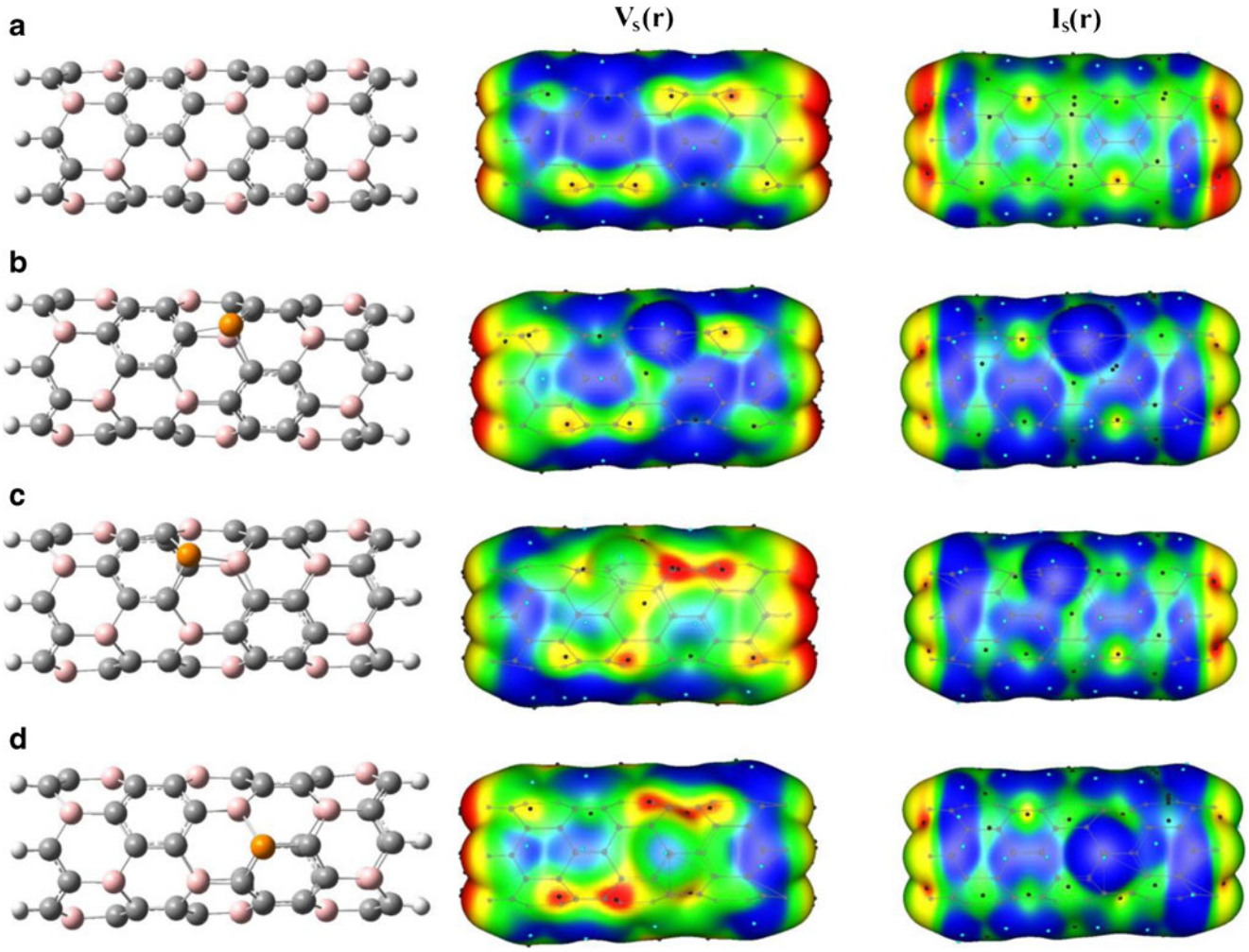

Fig. 2 Computed surface electrostatic potentials [$V_S(\mathbf{r})$] and average local ionization energies [$\bar{I}_S(\mathbf{r})$] for different models of (6,0) BC3NTs. Color range (in kcal mol^{-1}) for $V_S(r)$: *red* > 12.7, 4.6 < *yellow* < 12.7, −3.6 < *green* < 4.6, and *blue* < −3.6. Color range for $I_S(r)$ (in eV) is: *red* > 12.6, 11.3 < *yellow* < 12.6, 9.9 < *green* < 11.3, and *blue* < 9.9. The *black* and *blue* points refer to surface maxima and minima, respectively. **a** Pristine, **b** P_{B7}, **c** P_{C6} and P_{C8}

surface. In each P-doped tube studied, phosphorus preserves its sp^3 character, and bonds with tetrahedral-like configurations, with bond angles close to 101°. The P–C and P–B bond distances are about 1.85 and 1.87 Å, which are quite large compared to 1.42 Å for C–C sp^2 bonds. The larger bond lengths, combined with the difference in bond angles, force P to protrude from the nanotube surface, displacing also the positions of the first- and second-neighbors out of the plane (see Fig. 2).

Recent studies have proven electrostatic potential quantities to be suitable parameters with which to study the electronic structure of different nanotubes [39–45]. The computed surface electrostatic potentials of the (6,0) BC3NTs are presented in Fig. 2. For each zigzag BC3NT model studied, Table 1 also gives the positive and negative surface areas, A_S^+ and A_S^-, and the properties of the surface electrostatic potential as discussed in "Computational aspects". In the case of the pristine (6,0) BC3NT, the electron-donating hydrogens cause the outer carbon surfaces to become negative, with $V_{S,min}$ about −12 kcal mol^{-1}. The inside of the tube is positive, with maxima $V_{S,max}$ about +1 kcal mol^{-1}. However, the overall $Vs(\mathbf{r})$ surface is negative, $A_S^- > A_S^+$. The most negative regions are associated with the capped carbon sites (C1 and C12), the $V_{S,min}$ are about −12 kcal mol^{-1}, i.e., weaker than those of zigazag (6,0) CNT [42]. Looking at Fig. 2a, it is evident that the most positive regions are associated with the hydrogen atoms located at tips; the $V_{S,max}$ are about 21 kcal mol^{-1}, greater that those of ethylene (ca. 11 kcal mol^{-1}) and benzene (ca. 12 kcal mol^{-1}). These positive outer surfaces are due to the electronic charge withdrawn from hydrogens by carbon atoms. We note that there are also weak positive regions above boron atoms. These $V_{S,max}$ represent attractive channels for the approach of a nucleophile to the surface of a zigzag BC3NT. The value of Π, which implies an internal charge separation, is calculated to be 7 kcal mol^{-1}, which is in good agreement with reported values for pristine (5,5) and

Table 1 Computed surface electrostatic potentials and average local ionization energy of (6,0) and (4,4) BC3NTs[a,b,c]

Nanotube	A_S^+	A_S^-	$\overline{V}_S^+$	$\overline{V}_S^-$	σ^2_{total}	Π	$V_{S,max}$	$V_{S,min}$	$\bar{I}_{S,max}$	$\bar{I}_{S,min}$
(6,0)										
Pristine	271	283	8.0	−6.0	68	7.0	21.1	−11.8	13.2	7.8
P_{B7}	274	286	8.0	−5.8	69	7.0	19.7	−18.8	13.4	7.4
P_{C6}	291	272	7.8	−5.6	66	6.8	22.4	−14.1	13.4	7.6
P_{C8}	289	272	7.7	−5.4	63	6.6	21.3	−14.1	13.5	7.6
(4,4)										
Pristine	395	363	7.7	−4.5	54	6.2	21.1	−11.7	14.0	8.6
P_{B7}	404	359	7.7	−4.5	54	6.2	22.0	−16.8	14.0	7.5
P_{C6}	404	307	7.8	−4.5	55	6.3	21.5	−13.1	14.0	7.6
P_{C8}	408	356	7.6	−4.4	53	6.2	21.4	−13.9	14.0	7.8

A_S^+ and A_S^- are referred to the positive and negative surface area, respectively

All A_S^+ and A_S^- values in Å^2, whereas the evaluated $\overline{V}_S^+$, $\overline{V}_S^-$, σ^2_{total}, Π, $V_{S,max}$ and $V_{S,min}$ quantities in kcal mol^{-1}

$\bar{I}_{S,max}$ and $\bar{I}_{S,min}$ values in eV

(6,1) CNTs [39]. On the other hand, the greater variation in the surface potential of the pristine BC3NT can be seen in the magnitude of σ^2_{total}, which is distinctly larger than those of closed CNTs [40].

The results in Table 1 indicate that the evaluated surface quantities detect the effects of P-doping in the investigated structures. Moreover, the obtained magnitudes of surface minima reveal that the surface reactivities of the P_{C6} and P_{C8} zigzag BC3NTs are smaller than those of P_{B7} doped one. This trend means that the surface reactivity of the P_{B7} model of zigzag BC3NT detects more changes with respect to the P_{C6} and P_{C8} due to the phosphorous impurity. In the P_{B7} model, where one B atom is replaced by a single P atom, the negative regions associated with the carbon atoms are stronger than before, −12.6 vs −11.8 kcal mol^{-1}, while the positive ones of the inner surfaces are notably weaker. A general feature of the systems considered here is that the magnitudes of $V_{S,min}$ associated with carbon atoms tend to be stronger when carbon atoms are substituted with phosphorous atoms. In comparison with the pristine tube, the $V_{S,max}$ parameter for hydrogen atoms of the doped models do not detect any significant changes, while the $V_{S,max}$ parameters associated with the boron atoms are changed slightly. The lesser variation in the surface potential of the P_{C8} model can be seen in the magnitude of σ^2_{total}, which is now slightly smaller than for the P_{B7} and P_{C6}. It should be noted in Fig. 2 that there are some negative spots; these are all associated with the doped phosphorous atom, and range from −1 to −19 kcal mol^{-1}. The relatively larger surface potentials associated with the P atom can be attributed to its relatively larger atomic size.

Another local property that has often been used to study surface reactivity is the $\bar{I}_S(\mathbf{r})$, defined by Eq. (2). Figure 2a presents the $\bar{I}_S(\mathbf{r})$ plotted on the 0.001 au molecular surface of the pristine (6,0) BC3NT. As is evident, there are many $\bar{I}_{S,min}$ and $\bar{I}_{S,max}$ on the surface of the pristine tube; these are associated mainly with carbon and boron atoms, respectively. Looking at Fig. 2a, it is evident that the carbon itself has very reactive electrons, as depicted by the relatively low $\bar{I}_{S,min}$ values. The lowest of these are associated with the carbon framework as those located at the tips; these $\bar{I}_{S,min}$ have values about 7.8 eV (Table 2). These sites, thus, correspond to the least tightly held electrons, which should be the sites most reactive to electrophilic or to free radical attack. A particularly noteworthy observation is that the highest $\bar{I}_{S,max}$ are associated with the hydrogen atoms, with $\bar{I}_{S,max}$ between 12.8 and 13.2 eV. These calculated $\bar{I}_{S,max}$ values are slightly less than those of pristine (6,0) CNT (ca. 13.6 eV) and BNNT (ca. 14.2 eV) [42].

A quick look at the results of Table 1 indicates that the $\bar{I}_S(\mathbf{r})$ parameters detect the presence of dopant in zigzag BC3NT structures. Our results reveal that the phosphoros impurity tends to activate the surface toward electrophilic/radical attack. In the model P_{B7}, the value of $\bar{I}_{S,max}$ reduces by a magnitude of 0.4 eV with respect to the pristine tube (Table 1). This is due to the lower ionization energy of the phosphorous atom compared to carbon. The calculated $\bar{I}_{S,max}$ values of the P_{B7}, P_{C6} and P_{C8} models are 7.4, 8.0 and 8.2 eV, respectively. This different reactivity pattern between the BC3NT doped at B7, C6 and C8 sites can be attributed to the different contribution of electron pairs of the P atom to form a delocalized conjugated system with the adjacent sp^2-hybridized network. According to Fig. 2, the $\bar{I}_S(\mathbf{r})$ results suggest that activation of adjacent carbon/boron sites are quite localized for the each tube. Such a localized effect upon reactivity is consistent with

Table 2 Calculated reaction energies for a single hydrogen atom and H^+ ion adsorption on different sites of pristine (6,0) and (4,4) single-walled BC3 nanotubes (BC3NTs)

Site	$V_{S,min}$(kcal mol^{-1})	$\bar{I}_{S,min}$ (eV)	$\Delta E_{int}^{H\ radical\cdot}\ (kcal\ mol^{-1})$	$\Delta E_{int}^{H^+\ ion\cdot}\ (kcal\ mol^{-1})$
(6,0) BC3NT				
C1	−11.8	7.8	−81.5	−236.4
C3	−10.1	8.6	−49.2	−200.5
C4	−10.4	8.7	−46.6	−212.2
C5	−8.2	9.0	−37.1	−180.0
C6	−11.3	8.5	−49.1	−218.8
C8	−8.3	9.0	−37.1	−185.3
C9	−10.5	8.7	−46.6	−214.4
C11	−11.5	8.0	−69.3	−220.2
C12	−11.8	7.8	−81.5	−236.4
(4,4) BC3NT				
C1	−11.6	8.6	−74.4	−225.3
C2	−10.6	8.8	−66.7	−209.4
C4	−8.8	9.2	−44.6	−190.1
C5	−8.5	9.4	−40.4	−178.9
C6	−8.0	9.5	−36.2	−170.3
C8	−8.8	9.3	−44.1	−188.2
C9	−10.1	9.0	−49.8	−200.5
C10	−10.1	8.9	−52.5	−204.0
C12	−11.7	8.6	−76.1	−228.7

what was found earlier in the case of the Stone–Wales defect-containing [44] and chlorinated (5,5) armchair SWCNT [45].

(4,4) armchair BC3 nanotubes

Using B3LYP/6-31G* method in GAMESS, we have been able to converge all-electron DFT structures, with optimization of all structural degrees of freedom. Figure 3 indicates the optimized structures for the different models of armchair (4,4) BC3NT. The structural effects of P-doping of the metallic armchair (4,4) BC3NT, are very similar to that of the zigzag nanotube. The results indicate that the B–C bonds of the pristine armchair nanotube are slightly longer than those found in the zigzag one, being 1.42 Å for diagonal and 1.43 Å for tangential bonds. Similar to the zigzag case, doping with phosphorus causes a significant distortion in the armchair tube. However, the effects of P-doping on the geometries of the armchair models are less pronounced than those of the zigzag models. Parallel to the data of the zigzag BC3NTs, the results indicate that phosphorus preserves its sp^3 character, and bonds with tetrahedral-like configurations, with bond angles close to 98°. For each P-doped model considered, the distortion of the nanotube structure is limited primarily to the first-neighbors, with only a small displacement for the second-neighbors, while the third-neighbors are almost unchanged. The tube diameter at the defect site is about 6.8 Å, and the phosphorus atom protrudes outwardly from the nanotube. For a given doped configuration, the C–P and B–P bonds of the armchair tube are slightly shorter than those found in the zigzag one.

The evaluated surface $V_S(\mathbf{r})$ quantities for the optimized structure of pristine (4,4) BC3NT are listed in Tables 1. Unlike the zigzag nanotube, the entire surfaces, both inner and outer, are now positive $A_S^+ > A_S^-$, but only weakly so: $\overline{V}_S^+ = 7.7$ kcal mol^{-1} and $\overline{V}_S^- = -4.5$ kcal mol^{-1}. On the outer lateral surfaces of the tube, the positive regions above the borons are stronger than the negative ones of the carbons. One can see that the most positive regions are associated with boron atoms located at the tips—the $V_{S,max}$ are about 21 kcal mol^{-1}, greater that those of pristine (6,0) BNNT [42]. Note that there are also weak positive regions above and below the rings, due to the delocalized π electrons, as well as some strong ones associated with the hydrogen atoms. These $V_{S,max}$ values correspond to the attractive channels for the approach of a nucleophile to the surface of the nanotube. According to Fig. 3a, the most negative $V_{S,min}$ values of the pristine (4,4) BC3NT are associated with the capped carbons, and are fully consistent with the known tendency of electrophiles to react with these sites. Note also that, for the pristine armchair tube, the dominant theme, especially in side walls, is near-zero weakness and softness, showing relatively little variation (σ^2_{total} =54 kcal mol^{-1}) and small Π value.

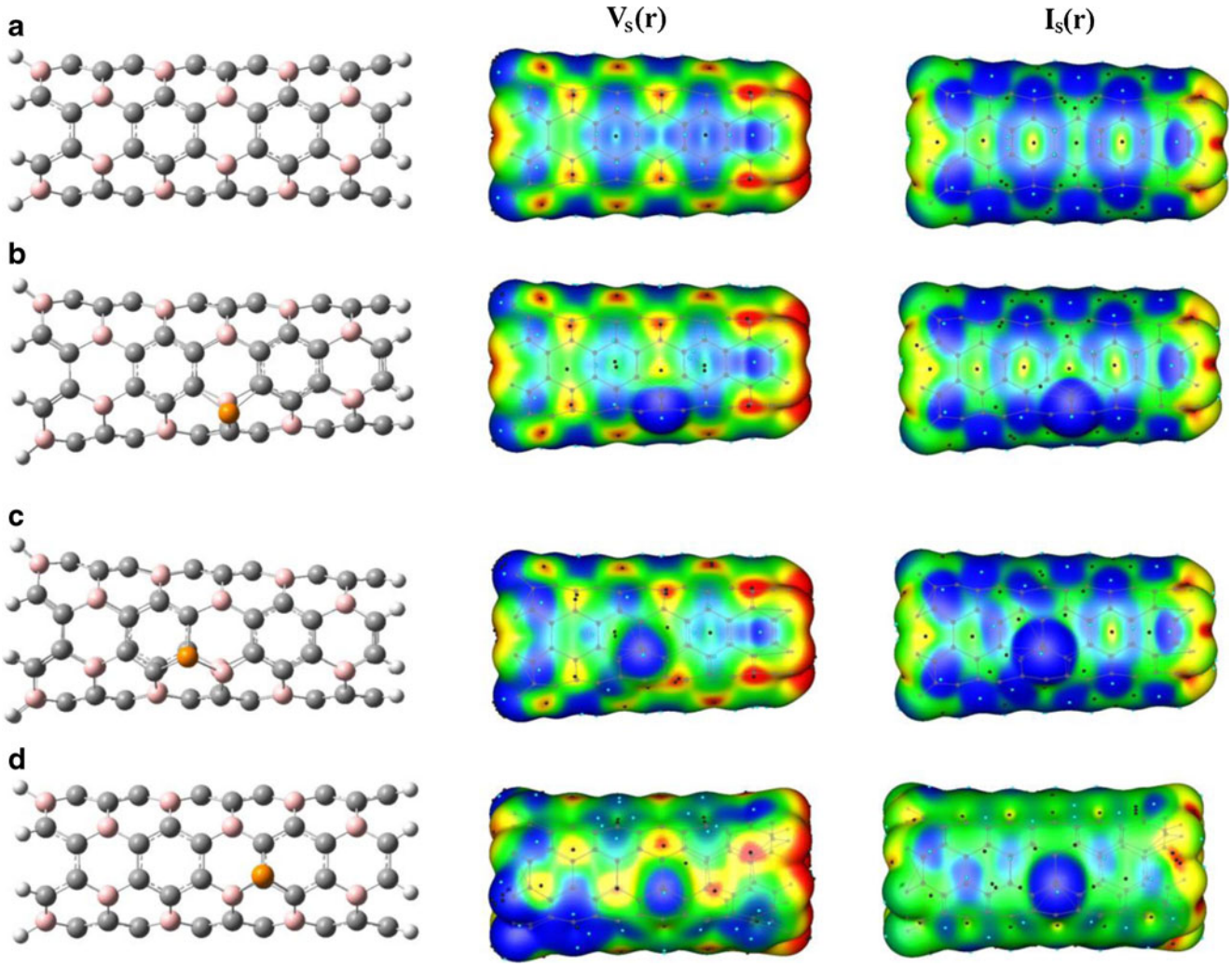

Fig. 3 Computed $V_S(\mathbf{r})$ and average $\bar{I}_S(\mathbf{r})$ for different models of (4,4) BC3NT. Color range (in kcal mol^{-1}) for $V_S(r)$ is: *red* > 12.7, 4.6 < *yellow* < 12.7, −3.6 < *green* < 4.6, and *blue* < −3.6. Color range for $I_S(r)$ (in eV) is: *red* > 12.6, 11.3 < *yellow* < 12.6, 9.9 < *green* < 11.3, and *blue* < 9.9. The *black* and *blue* points refer to surface maxima and minima, respectively. **a** Pristine, **b** P_{B7}, **c** P_{C6} and P_{C8}

The computed $V_S(\mathbf{r})$ on the side of the P-doped BC3NTs are quite different than those of the pristine one. Comparison with the $V_{S,min}$ of the pristine (4,4) nanotube indicates that the surface reactivity of the pristine tube is modified slightly after the phosphorus insertion. As in the case of pristine model, the overall surface is predominantly positive for the all P-doped models. We note that, due to the P-doping at boron or carbon site, the negative regions associated with adjacent carbon atoms are stronger than before. This notable increase in $V_{S,min}$ values of carbon atoms regarding the pristine model indicates the stronger tendency of the carbon atoms of the doped models to be susceptible to nucleophilic attack than those of the pristine one. Moreover, the most negative $V_{S,min}$ value of P_{B7}, predicted to indicate the most reactive site, is associated with the phosphorous atom with $V_{S,min}$=−16.8 kcal mol^{-1}. The corresponding $V_{S,min}$ values of P_{C6} and P_{C8} models are calculated to be −10.8 and −8.8 kcal mol^{-1}, respectively. On the other hand, the positive regions above the borons are stronger than before, at 21.4 to 22.0 kcal mol^{-1}. However, comparing the P-substituted models of zigzag and armchair BC3CNTs indicates that the properties of zigzag models detect the effects of P-doping more than armchair ones.

More interesting are the average local ionization energies on the armchair BC3NTs surfaces. Of primary interest are the magnitudes and locations of the lowest values of $\bar{I}_S(\mathbf{r})$, the local minima $\bar{I}_{S,min}$. These reveal the least tightly held, most reactive electrons, which should be the sites most favored to electrophilic or to free radical attack. For the pristine armchair tube, the lowest $\bar{I}_{S,min}$ are associated with capped carbon atoms, as can be seen very clearly in Fig. 3a. Moreover, a particularly interesting finding is that the sites of the lowest $\bar{I}_{S,min}$ in the pristine BC3NT are associated with the highest occupied molecular orbital (HOMO) [52]. This emphasizes the complementarity of the use of both frontier molecular

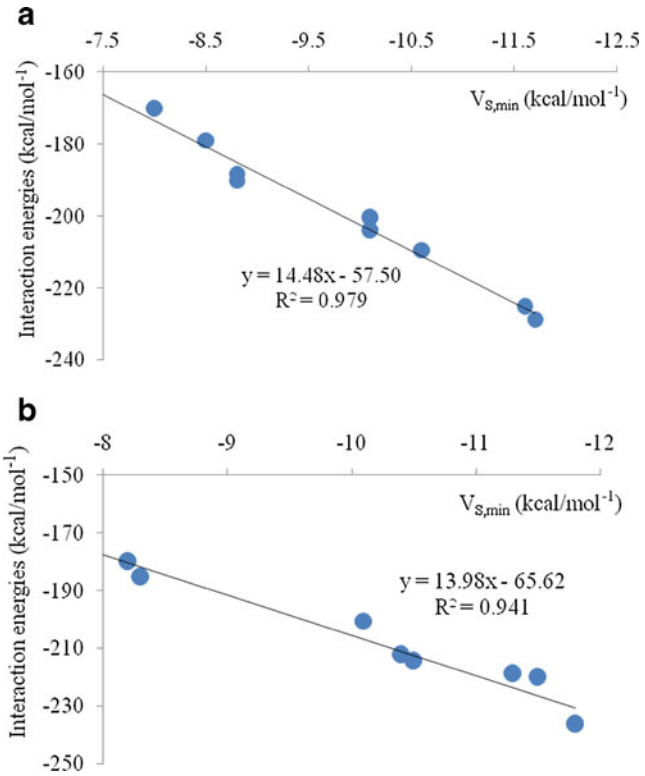

Fig. 4 Correlation between the calculated interaction energies (B3LYP/6-31G*) and predicted $V_{S,min}$ values of pristine **a** (6,0) and **b** (4,4) BC3NTs

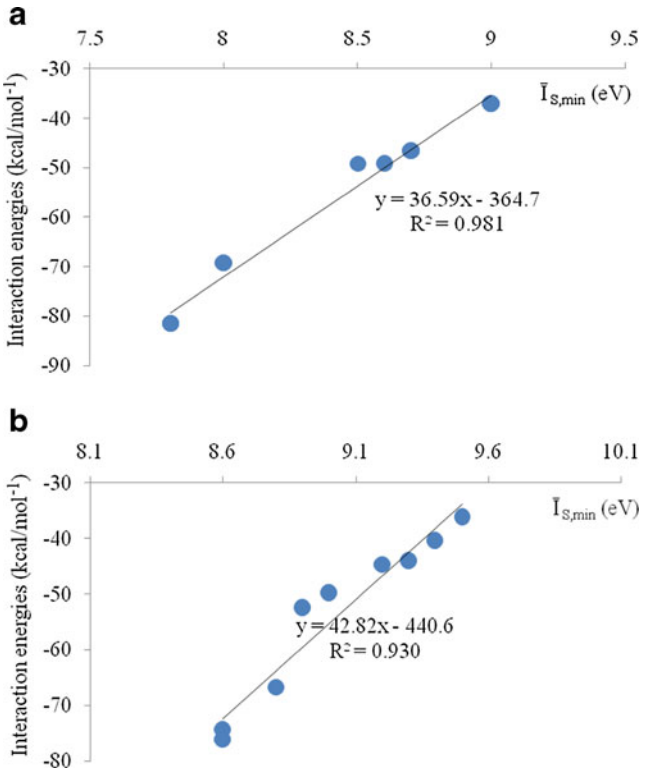

Fig. 5 Correlation between the calculated interaction energies (B3LYP/6-31G*) and predicted $\bar{I}_{S,min}$ values of pristine **a** (6,0) and **b** (4,4) BC3NTs

orbital approach and $\bar{I}_{S,min}$ to predict the reactivity of BC3NT. The evaluated $\bar{I}_{S,max}$ values in Fig. 3a are about 14 eV and are associated mostly with hydrogen and boron atoms.

From the results in Table 1, it is apparent that the surface reactivity of the BC3NT exhibits dramatic changes before and after doping with the P atom. What is notable, however, is the significant reduction in $\bar{I}_{S,min}$ of the three neighboring carbons in the P_{B7} model. These carbons are accordingly activated relative to pristine BC3NT, which can presumably be attributed to their having acquired some radical character. The remaining interior carbons, however, retain approximately the $\bar{I}_{S,min}$ that they had in the pristine tube. In addition, the significant decrease in the $\bar{I}_{S,min}$ value of the P_{B7} model regarding the pristine model stands for the stronger tendency of its phosphorous site to attract electrophilic/free radical attack than those of P_{C6} and P_{C8} models. So we believe that doping BC3NTs with P may be a good method for improving their surface reactivities. For the doped P_{C6} or P_{C8} models, the P impurity can also significantly improve the tube's surface reactivity and it allows their surface properties to be controlled.

Interaction energies

In order to verify the surface reactivity pattern based on the chosen reactivity descriptors discussed above, we have calculated the reaction energies for the interaction of an H^+ ion or H radical with external surface of the (6,0) and (4,4) BC3NTs. The evaluated reaction energies (at the B3LYP/6-31G* level of theory) are listed in Table 2. It is clearly seen that, for each nanotube studied, the reaction energies predict the reactive sites as that of the $V_{S,min}$ and $\bar{I}_{S,min}$ values. As anticipated, according to reaction energies, the capped carbon atoms are highly reactive sites for atomic hydrogen chemisorptions. The interaction energies become more negative (more stabilizing) as $V_{S,min}$ increases (indicating increasing reactivity). The strongest interaction, however, is with the capped carbon atoms. Figures 4 and 5 show the correlation between the calculated interaction energies with the predicted $V_{S,min}$ and $\bar{I}_{S,min}$ values at the sites of carbon atoms. We found an acceptable correlation for each case, indicating that $V_{S,min}$ and $\bar{I}_{S,min}$ provide an effective means for rapidly and economically assessing the relative reactivities of finite-sized BC3NTs.

Conclusions

This work investigated the geometries and electronic structure of pristine and P-doped (6,0) zigzag as well as (4,4) armchair BC3NTs. Geometry optimizations indicated that the shape of the cross-section of P-doped nanotubes changes from circular to slightly oval, and the phosphorus atom protrudes outwardly

from the nanotube surface. Moreover, the phosphorus atom still tends to form sp^3 bonding, and doping with phosphorus causes large distortions in the nanotubes. For each nanotube studied, surface electrostatic potentials and average local ionization energies were calculated. It is found that the characteristic surface patterns and evaluated surface quantities are influenced considerably by P-doping. Due to P-doping at the boron or carbon sites of pristine BC3NTs, the negative regions associated with carbon atoms are stronger than before. Furthermore, the phosphorous atom in the all P-doped model tends to activate the carbon site toward electrophilic or to free radical attack. However, comparing the P-substituted models of zigzag and armchair BC3CNTs indicate that the properties of zigzag models detect the effects of P-doping more than armchair models. An acceptable correlation between the calculated interaction energies with the predicted $V_{S,min}$ and $\bar{I}_{S,min}$ values at the sites of carbon atoms was found. This indicates that $V_S(\mathbf{r})$ and $\bar{I}_{S,min}$ provide an effective means for rapidly and economically assessing the relative reactivities of finite-sized BC3NTs.

References

1. Dinadayalane TC, Leszczynski J (2010) Remarkable diversity of carbon–carbon bonds: structures and properties of fullerenes, carbon nanotubes, and graphene. Struct Chem 21:1155–1169
2. Saha S, Dinadayalane TC, Leszczynska D, Leszczynski J (2012) Open and capped (5,5) armchair SWCNTs: a comparative study of DFT-based reactivity descriptors. Chem Phys Lett 541:85–91
3. Nojeh A, Lakatos GW, Peng S, Cho K, Pease RFW (2003) A carbon nanotube cross structure as a nanoscale quantum device. Nano Lett 3: 1187–1190
4. Wang Y, Shao Y, Matson DW, Li J, Lin Y (2010) Nitrogen-doped graphene and its application in electrochemical biosensing. ACS Nano 4:1790–1798
5. Cruz-Silva E, López-Urías F, Muñoz-Sandoval E, Sumpter BG, Terrones H, Charlier JC, Meunier V, Terrones M (2010) Electronic transport and mechanical properties of phosphorus- and phosphorus nitrogen-doped carbon nanotubes. ACS Nano 3:1913–1921
6. Mykhailenko O, Matsui D, Prylutskyy Y, Le Normand F, Eklund P, Scharff P (2007) Monte Carlo simulation of intercalated carbon nanotubes. J Mol Model 13:283–287
7. Nikitin A, Li X, Zhang Z, Ogasawara H, Dai H, Nilsson A (2008) Hydrogen storage in carbon nanotubes through the formation of stable CH bonds. Nano Lett 8:162–167
8. Chen P, Wu X, Lin J, Tan K (1999) High H_2 uptake by alkali-doped carbon nanotubes under ambient pressure and moderate temperatures. Science 285:91–93
9. Pan X, Fan Z, Chen W, Ding Y, Luo H, Bao X (2007) Enhanced ethanol production inside carbon-nanotube reactors containing catalytic particles. Nat Mater 6:507–511
10. Wang Z, Jia R, Zheng J, Zhao J, Li L, Song J, Zhu Z (2011) Nitrogen-promoted self-assembly of N-doped carbon nanotubes and their intrinsic catalysis for oxygen reduction in fuel cells. ACS Nano 5: 1677–1684
11. Gong K, Du F, Xia Z, Durstock M, Dai L (2009) Nitrogen-doped carbon nanotube arrays with high electrocatalytic activity for oxygen reduction. Science 323:760–764
12. Yang S, Zhao G, Khosravi E (2010) First principles studies of nitrogen doped carbon nanotubes for dioxygen reduction. J Phys Chem C 114:3371–3375
13. Xu X, Jiang S, Hu Z, Liu S (2010) Nitrogen-doped carbon nanotubes: high electrocatalytic activity toward the oxidation of hydrogen peroxide and its application for biosensing. ACS Nano 4:4292–4298
14. Cruz-Silva E, López-Urías F, Munõz-Sandoval E, Sumpter BG, Terrones H, Charlier JC, Meunier V, Terrones M (2009) Electronic transport and mechanical properties of phosphorus- and phosphorus nitrogen-doped carbon nanotubes. ACS Nano 3:1913–1921
15. Guo H, Kumar S, Hauge RH, Smalley RE (2004) Polyacrylonitrile single-walled carbon nanotube composite fibers. Adv Mater 16:58–61
16. Panchakarla LS, Govindaraj A, Rao CNR (2007) Nitrogen- and boron-doped double-walled carbon nanotubes. ACS Nano 1:494–500
17. Miyamoto Y, Rubio A, Louie SG, Cohen ML (1994) Electronic properties of tubule forms of hexagonal BC3. Phys Rev B 50: 18360–18366
18. Su WS, Chang CP, Li MF, Li TL (2011) Electronic structures and work functions of BC3 nanotubes: a first-principle study. J Appl Phys 110:014312
19. Tománek D, Wentzcovitch RM, Louie SG, Cohen ML (1988) Calculation of electronic and structural properties of BC3. Phys Rev B 37:3134–3136
20. Wang Q, Chen LQ, Annett JF (1996) Stability and charge transfer of C3B ordered structures. Phys Rev B 54:R2271–R2275
21. Fuentes GG, Borowiak-Palen E, Knupfer M, Pichler T, Fink J, Wirtz L, Rubio A (2004) Formation and electronic properties of BC3 single-wall nanotubes upon boron substitution of carbon nanotubes. Phys Rev B 69:245403
22. Borowiak-Palen E, Rümmeli M, Gemming T, Knupfer M, Kalenczuk RJ, Pichler T (2005) Formation of novel nanostructures using carbon nanotubes as a frame. Synth Metal 153:345–348
23. Tanaka H, Kawamata Y, Simizu H, Fujita T, Yanagisawa H, Otani S, Oshima C (2005) Novel macroscopic BC3 honeycomb sheet. Solid State Commun 136:22–25
24. Heṁandez E, Goze C, Bernier P, Rubio A (1998) Elastic properties of C and $B_xC_yN_z$ composite nanotubes. Phys Rev Lett 80:4502–4505
25. Ren X, Chen C, Nagatsu M, Wang X (2011) Carbon nanotubes as adsorbents in environmental pollution management: a review. Chem Eng J 170:395–410
26. Zhao J, Buldum A, Han J, Lu JP (2002) Gas molecule adsorption in carbon nanotubes and nanotube bundles. Nanotechnology 13(2): 195–200
27. Shirvani BB, Beheshtian J, Esrafili MD, Hadipour NL (2010) DFT study of NH_3 adsorption on the (5,0), (8,0), (5,5) and (6,6) single-walled carbon nanotubes calculated binding energies, NMR and NQR parameters. Phys B 405:1455–1460
28. Frank B, Zhang J, Blume R, Schlüogl R, Su D (2009) Heteroatoms increase the selectivity in oxidative dehydrogenation reactions on nanocarbons. Angew Chem Int Ed 48:6913–6917
29. Ayala P, Arenal R, Rüummeli M, Rubio A, Pichler T (2010) The doping of carbon nanotubes with nitrogen and their potential applications. Carbon 48:575–586
30. Lin YH, Lu F, Tu Y, Ren ZF (2004) Glucose biosensors based on carbon nanotube nanoelectrode ensembles. Nano Lett 4:191–195
31. Naray-Szabo G, Ferenczy GG (1995) Molecular electrostatics. Chem Rev 95:829–847
32. Sauer J, Ugliengo P, Garrone E, Saunders VR (1994) Theoretical study of van der Waals complexes at surface sites in comparison with the experiment. Chem Rev 94:2095–2160
33. Bulat FA, Toro-Labbé A, Brinck T, Murray JS, Politzer P (2010) Quantitative analysis of molecular surfaces: areas, volumes, electrostatic potentials and average local ionization energies. J Mol Model 16:1679–1691

34. Murray JS, Peralta-Inga Z, Politzer P (2000) Computed molecular surface electrostatic potentials of the nonionic and zwitterionic forms of glycine, histidine, and tetracycline. Int J Quantum Chem 80:1216–1223
35. Politzer P, Murray JS, Concha MC (2007) Halogen bonding and the design of new materials: organic bromides, chlorides and perhaps even fluorides as donors. J Mol Model 13:643–650
36. Riley KE, Murray JS, Politzer P, Concha MC, Hobza P (2009) Br··· O complexes as probes of factors affecting halogen bonding: interactions of bromobenzenes and bromopyrimidines with acetone. J Chem Theory Comput 5:155–163
37. Esrafili MD (2012) Investigation of H-bonding and halogen-bonding effects in dichloroacetic acid: DFT calculations of NQR parameters and QTAIM analysis. J Mol Model 18:5005–5016
38. Esrafili MD (2013) A theoretical investigation of the characteristics of hydrogen/ halogen bonding interactions in dibromo-nitroaniline. J Mol Model 19:1417–1427
39. Peralta-Inga Z, Lane P, Murray JS, Boyd S, Grice ME, O'Connor CJ, Politzer P (2003) Characterization of surface electrostatic potentials of some (5,5) and (n,1) carbon and boron/nitrogen model nanotubes. Nano Lett 3:21–28
40. Politzer P, Lane P, Murray JS, Concha MC (2005) Comparative analysis of surface electrostatic potentials of carbon, boron/nitrogen and carbon/boron/nitrogen model nanotubes. J Mol Model 11:1–7
41. Politzer P, Murray JS, Lane P, Concha MC, Jin P, Peralta-Inga Z (2005) An unusual feature of end-substituted model carbon (6,0) nanotubes. J Mol Model 11:258–264
42. Esrafili MD, Behzadi H (2013) A comparative study on carbon, boron-nitride, boron-phosphide and silicon-carbide nanotubes based on surface electrostatic potentials and average local ionization energies. J Mol Model 19:2375–2382
43. Esrafili MD (2013) Nitrogen-doped (6, 0) carbon nanotubes: a comparative DFT study based on surface reactivity descriptors. Comput Theor Chem 1015:1–7
44. Dinadayalane TC, Murray JS, Concha MC, Politzer P, Leszczynski J (2010) Reactivities of sites on (5,5) single-walled carbon nanotubes with and without a Stone-Wales defect. J Chem Theory Comput 6:1351–1357
45. Saha S, Dinadayalane TC, Murray JS, Leszczynska D, Leszczynski J (2012) Surface reactivity for chlorination on chlorinated (5,5) armchair SWCNT: a computational approach. J Phys Chem C 116:22399–22410
46. Schmidt MW, Baldridge KK, Boatz JA, Elbert ST, Gordon MS, Jensen JH, Koseki S, Matsunaga N, Nguyen KA, Su SJ, Windus TL, Dupuis M, Montgomery JA (1993) General atomic and molecular electronic structure system. J Comput Chem 14:1347–1363
47. Politzer P, Murray JS, Sen KD (1996) Molecular electrostatic potentials: concepts and applications. Elsevier, Amsterdam
48. Sjoberg P, Murray JS, Brinck T, Politzer P (1990) Average local ionization energies on the molecular surfaces of aromatic systems as guides to chemical reactivity. Can J Chem 68:1440–1443
49. Politzer P, Murray JS, Bulat FA (2010) Average local ionization energy: a review. J Mol Model 16:1731–1742
50. Politzer P, Murray JS, Peralta-Inga Z (2010) Molecular surface electrostatic potentials in relation to noncovalent interactions in biological systems. Int J Quantum Chem 85:676–684
51. Brinck T, Murray JS, Politzer P (1992) Quantitative determination of the total local polarity (charge separation) in molecules. Mol Phys 76:609–617
52. Esrafili MD (2013) Electronic structure and surface reactivity of BC3 nanotubes from first-principle calculations. Struct Chem. doi:10.1007/s11224-013-0269-2